# Transmission Lines, Single-Sideband Mixers and the 21-cm line

Niels Joubert

April 12, 2007[1]
http://ugastro.berkeley.edu/~njoubert/

## ABSTRACT

This lab report covers several overlapping topics and concludes with observations of the 21-cm Hydrogen line. We examine transmission lines and waveguides to further our knowledge of the electronics we need to do our observations with. We demonstrated the importance of impedance matching by measuring standing wave ratios in excess of 3 for a mismatched load on a slotted line, versus the much more acceptable ratio of 1.5 for a matched load. We found that the propagation speed of signals through a normal coax is only about $\frac{3}{4}c$, an important fact in designing equipment that demands certain phase shifts to be introduced by cables. Waveguides revealed their cut-off frequency that is related to the width of the waveguide according to $2a$, and their SWR and propagation characteristics. We then studied mixers, and found that Fourier transforms has a limit on the frequency resolution that we can resolve, and leakage power obstructs frequencies closer spaced than $\frac{1}{T}$ where T is the sampling period. We demonstrated that the ambiguity in frequency value disappears when we use single sideband mixers, so that we can resolve a signal to exactly which sideband it is in and what its frequency is. We then used our new-found electronics knowledge to study the 21-cm line, creating a calibrated spectrum of the Hydrogen at one location in our galactic plane, and finding that the gas we observed is moving away from us at approximated 6 $kms^{-1}$

---

[1]Document created Saturday, March 17, 2007

**Contents**

## 1. INTRODUCTION

The third lab of the Undergraduate Radioastronomy Laboratory course covered a diverse set of experiments and information that is important in observations and data-analysis as a radio astronomer. Starting with the transmission of signals, this lab included several bench experiments to study the propagation of electromagnetic waves through coax, waveguides and our signal path. We moved on to discuss double-sideband mixers and their ability to distinguish the upper and lower sidebands in an incoming signal. We used these mixers in the signal path of our Horn experiment, where we observed the 21-cm Hydrogen line. We studied the hydrogen line's spectrum, and calibrated it both for intensity (in terms of temperature) and Doppler velocity (in terms of km s$^{-1}$).

## 2. TRANSMISSION LINES, WAVEGUIDES, IMPEDANCE MATCHING

### 2.1. Introduction

So far we have blindly accepted that signals somehow enter our antenna and move through the multitude of transmission lines that make up our signal path. We have taken for granted the capability of these passive elements - our transmission lines. We will now study the properties of these crucial elements. The physics behind the workings of these innocent-looking components befit the proverb that there is more than meets the eye! We will study reflection, wave speed and impedance in transmission lines, slotted lines and waveguides to further our knowledge of the workings of a signal path.

### 2.2. Slotted Line Coax Cable

Our first venture into the study of transmission lines is measuring wavelength and velocity in a slotted line apparatus. A slotted line allows us to measure the electric field strength through the length of this apparatus, which functions like a coaxial cable. To find the exact frequency of waves that we transmit into this device, we use a cavity wavemeter. The cavity wavemeter functions as an adjustable attenuator, removing a significant amount of the amplitude of the signal at a specific frequency. By adjusting it through the range of input frequencies, we can find the exact frequency of our signal entering the slotted line.

#### 2.2.1. Finding Wavelength and Propagation Velocity

To find the velocity in the slotted line, we need to find the wavelength of the specific frequency we are feeding into the line. We can exploit *standing waves* to find the wavelength by finding where the nodes (points of no signal strength) are inside the slotted line. Standing waves in a transmission line is caused by the interference of a forward-moving and a reflected wave to form a wave that appears to be stationary in the medium. The nodes corresponds roughly to $\frac{1}{2}\lambda$, so we can find the wavelength from these node positions.

We execute two sightly different measurements of the node positions. First we leave the one end of the slotted line open, and measure the positions of the nodes from the start of the slotted line. We then short the end of the slotted line and make the same measurement, obtaining the following data:

| Node | Open Cable Nodes (cm) | Shorted Cable Nodes (cm) |
|------|-----------------------|--------------------------|
| 0    | 2.00                  | 3.60                     |
| 1    | 6.85                  | 8.50                     |
| 2    | 11.60                 | 13.30                    |
| 3    | 16.45                 | 18.05                    |
| 4    | 21.25                 | 22.90                    |
| 5    | 26.00                 | 27.70                    |
| 6    | 30.80                 | 32.50                    |
| 7    | 35.70                 | 37.30                    |
| 8    | 40.50                 | 42.10                    |
| 9    | 45.25                 | 46.9                     |
| 10   | 50.05                 | -                        |

We thus have 10 or 11 samples of data from our standing waves, with the distance between each point being roughly equal to a half wavelength. In an ideal setup, we would get perfect reflection and interference so that all these nodes are spaced by exactly $\frac{1}{2}\lambda$. In practice, we find that transmission lines are slightly lossy and outside noise sources can cause interference with our signals, so that the nodes are spaced slightly differently. The first method to find the "true" wavelength that comes to mind is that of averaging:

$$\frac{\sum x_{i+1} - x_i}{M - 1} = \frac{x_{M-1} - x_0}{M - 1} \tag{1}$$

Where $x_i$ is the position of null $i$ and $M$ is the total number of nulls. The problem with this averaging, as shown in equation 1, is that it is equal to disregarding all the intermediate points and using only the first and last sample. We definitely want to do better than this, and we can if we notice that the positions of the nulls are described by a simple linear relation:

$$x_m = A + m\frac{\lambda}{2} \tag{2}$$

We exploit this by using least-squares to fit a first-degree polynomial to our dataset. The coefficients generated by the fitting procedure will give us the value for $\frac{1}{2}\lambda$, and a error estimate for this value. We can use this to calculate the velocity of propagation very easily using introductory physics:

$$\nu = f * \lambda \tag{3}$$

Applying this to our data gives the following:

|              | Open Cable | Closed Cable |
|--------------|------------|--------------|
| $f$          | 3118 MHz   | 3118 MHz     |
| fitted $\lambda$ | 9.6109 cm | 9.6127 cm |
| $\sigma_\lambda$ | 0.03467 cm | 0.02938 cm |
| $\nu$        | 299 668 160 $m\,s^{-1}$ | 299 724 850 $m\,s^{-1}$ |
| $\sigma_\nu$ | 103 895 $m\,s^{-1}$ | 88 082 $m\,s^{-1}$ |

As we can see, the error estimates is small compared to the fitted values of $\lambda$ and $\nu$, and our velocities are close to the accepted value of 299 792 458 $m\,s^{-1}$.

### 2.2.2. Voltage Standing Wave Ratio and Impedance

We want to develop a quantitative concept of the standing waves in our transmission line. We start from the concept of a "voltage refection coefficient" - the ratio of reflected to passed-through waves. This value is related to the resistance $R_L$ of the load that terminates the cable, and the impedance $Z_0$ of the line.

$$\rho = \frac{V_R}{V_F} = \frac{R_L - Z_0}{R_L + Z_0} \tag{4}$$

Standing waves come from the interference of the forward and reflected waves. The maximum and minimum voltage through the cable is then given by

$$V_{max} = V_{forward} + V_{reflected} \tag{5}$$
$$V_{min} = V_{forward} - V_{reflected} \tag{6}$$

Through some mathematical ingenuity we find the value of the standing wave's voltage through adding the $V_{forward}$ and $V_{reflected}$ since they are related by equation 4. We finally use equation 4 again to relate $V_{max}$ and $V_{min}$ to $\rho$ so that we find the ratio between the maximum and minimum values of the standing wave. This is known as the *Voltage Standing Wave Ratio*

$$VSWR = \frac{|V_{max}|}{|V_{min}|} = \frac{1 + \rho}{1 - \rho} \tag{7}$$

We use the same setup as for measuring the nulls in the slotted line to measure the maximum and minimum voltages of the standing wave at several positions. We used two different loads on the end, one being a matched load that is close to the impedance of the cable. and an unmatched load that has a resistance quite different from the impedance of the cable.

| Load Resistance (Ohms) | $49.8\,\Omega$ | $75.5\,\Omega$ |
|---|---|---|
| Maximum $|V|$ (mV) | [34, 33, 32, 33] | [87, 85, 86] |
| Minimum $|V|$ (mV) | [28, 27, 26, 27] | [28, 27, 26] |

We find the VSWR for each pair of min/max values, and we average them to find the VSWR in the slotted line. We also use equation 7 to calculate the theoretical value of the $VSWR$:

| Load Resistance (Ohms) | $49.8\,\Omega$ | $75.5\,\Omega$ |
|---|---|---|
| Average VSWR | 1.22237 | 3.18766 |
| Expected VSWR | 1.002 | 1.5100 |

Unfortunately reality and our model does not exactly agree in this case. The differences in recorded and predicted VSWR is fairly big in this case, but it can be attributed to a number of factors. The measurement of the minimum and maximum voltage levels was by hand, reading off the oscilloscope. Also, the match could have appeared as a higher resistance than measured due to a bad connection in screwing the match onto the end of the slotted line. The important concept to see from this data is that the standing wave ratio is at its smallest when the load resistance and cable impedance is the same, so that we have a perfect match. This is crucial in all our electronics, since the useful data we can sample becomes progressively less as waves are reflected. A large VSWR ratio somewhere in your signal path can ruin a good measurement by attenuating the data we receive, throwing of calibrations and sensitive sampling equipment.

### 2.3. Flexible Coax at C-band

We found that velocity is independent of frequency for coax cables, and we measured the velocity of propagation in the slotted line. Although this was valuable to model the physics, we very rarely use slotted lines to connect equipment together. We now want to find the wavelength and velocity of EM waves in a flexible coax such as the transmission lines used to guide signals from the dish to our sampler. We cannot measure the node position inside the cable, since the cable is sealed, so we need to find some other way to measure wavelength and velocity. We have the following parameters and information with which we need to derive velocity and wavelength:

4

- *Information:* Velocity is independent of Frequency

- *Information:* Length of Cable = 855 cm

- *Parameter:* $\nu$ (We can vary frequency)

- *Equation:* $\nu = \lambda f$

- *Equation:* $L = n\frac{\lambda}{2}$

We use the slotted line at the beginning of the flexible coax to find a node point. We can now make two measurements by slowly varying the frequency until we have the next node at the same position - thus, we increased the total amount of nodes in the coax by 1. We measure the frequency of both these samples using the cavity wavemeter, and we have all the information to determine the velocity in the coax cable.

$$L \;=\; n\frac{\lambda_1}{2} \tag{8a}$$

$$L \;=\; (n+1)\frac{\lambda_2}{2} \tag{8b}$$

Since velocity is independent of frequency, we can write:

$$\lambda_1 \;=\; \frac{\nu}{f_1} \tag{9a}$$

$$\lambda_2 \;=\; \frac{\nu}{f_2} \tag{9b}$$

We combine and subtract these equations to find:

$$\nu = 2L(f_2 - f_1) \tag{10}$$

And so we find our final data:

| L | 855 cm |
|---|---|
| $f_2$ | 3043.6 MHz |
| $f_1$ | 3037.7 MHz |
| $f_2 - f_1$ | 6.1 MHz |
| $\nu$ | 0.73c |

It is very important to note that the propagation velocity inside the coax cable is about $\frac{3}{4}$ of of the speed of light in a vacuum. This is important if we want to use cables to create delays and phase shifts, which we will do in section 3.

### 2.4. Waveguides

Waveguides steer electromagnetic waves through a metal-enclosed empty region, allowing the wave to propagate through the empty space. They have several properties that differs from coax cables, which we probe here. First off we get an idea of the standing waves in the waveguide through measuring nodes in the waveguide, and calculating the VSWR value. We will then try to find the propagation velocity in the waveguide, and finally we will examine the theory that predicts a "cutoff wavelength" - a value for which longer waves will not be propagated at all.

#### 2.4.1. Standing Waves

We measure the VSWR when the end of the waveguide is open and shorted. We do this by moving a probe through it and recording all the local minima and local maxima voltage levels. We find the following data:

| Waveguide Configuration; | Open End | Closed End |
|---|---|---|
| Input Frequency (MHz) | 10494 MHz | 10494 MHz |
| Maximum $|V|$ (mV) | [ 96, 96, 96 ] | [ 140, 142, 143, 143 ] |
| Minimum $|V|$ (mV) | [ 58, 58, 58 ] | [ 2, 2, 1, 2 ] |

We find the VSWR for each pair of min/max values, and we average them to find the VSWR in the waveguide.

| Waveguide Configuration; | Open End | Closed End |
|---|---|---|
| Measured VSWR | 1.655 | 88.875 |

The VSWR values for the waveguide is quite different from the VSWR of a coax cable. We should expect this, since the end of the cable is completely open - there is no impedance and thus practically no reflected wave. On the other hand, when we close it using a solid metal barrier, we reflect a very large amount of the wave, so that the interference between the forward and reflected wave is almost completely constructive at is maximum and almost completely destructive at its minimum. This shows an interesting property of VSWR - as VSWR goes to infinity, you reflect all energy, while as it goes to 1, you pass all energy.

#### 2.4.2. Velocity in Waveguide

We want to examine the propagation velocity of waved in the waveguide. We take the experiment one step further than with coax cables by measuring nulls at multiple frequency values. We want to find the actual wavelength from the nulls in energy in the waveguide that we record. We do this in exactly the same way as we did in section 2.2.1, by fitting a first degree polynomial to our data. Once we have the wavelength, finding the velocity becomes trivial.

| Frequency $\nu$ (MHz) | Null Position (cm array) | Wavelength (cm) | Velocity $m\,s^{-1}$ |
|---|---|---|---|
| 8294 | [ 10.2, 12.84, 15.47 ] | 5.89 | $4.888 * 10^8$ |
| 8713 | [ 10.21, 12.84, 15.47 ] | 5.25 | $4.583 * 10^8$ |
| 9296 | [ 10.00, 12.28, 14.55, 16.80 ] | 4.53 | $4.214 * 10^8$ |
| 9792.5 | [ 9.40, 11.47, 13.55, 15.62, 17.79 ] | 4.18 | $4.099 * 10^8$ |
| 10296 | [ 8.91, 10.82, 12.71, 14.60, 16.46 ] | 3.77 | $3.887 * 10^8$ |
| 10739 | [ 8.29, 10.06, 11.82, 13.60, 15.35 ] | 3.52 | $3.789 * 10^8$ |

At first glance something seems drastically wrong - every calculated velocity exceeds the speed of light! This is not a contradiction of the laws of relativity, but rather reminds us that we are not necessarily

measuring *Group Velocity*[2], but we measure *Phase Velocity*, which can exceed the speed of light in certain cases. Information travel at the group velocity, thus no superluminal events occur when we measure these frequencies.
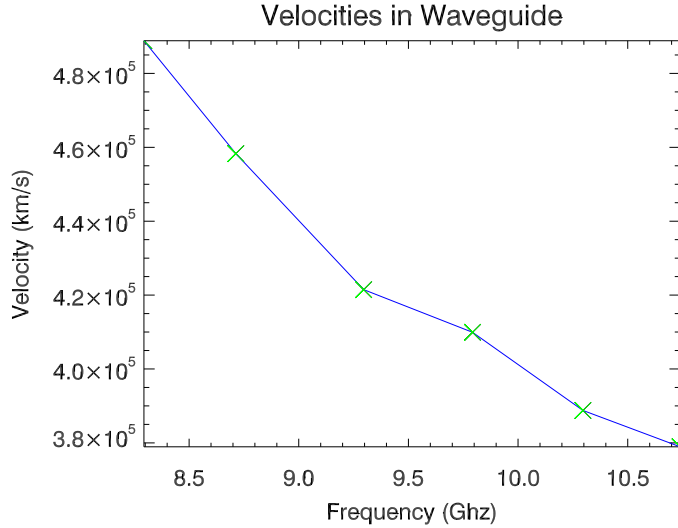


Fig. 1.— The measured phase velocity inside the waveguide.

Figure 1 shows the frequency of the signal propagating through the waveguide against the phase velocity. Notice how the velocity increases as the frequency decreases. This leads to the next characteristic of waveguides that we study - the cut-off frequency.

### 2.4.3. Cut-off frequency

We know that the frequency of the signal is fixed according to our signal generator. Since the velocity is significantly faster than the speed of light, the wavelength of waves in the waveguide naturally has to be longer. The "guide wavelength" is the wavelength inside the waveguide, and can be related to the free-space wavelength of the signal and the width of the waveguide (a):

$$\lambda_g = \frac{\lambda}{\left[1 - (\lambda/2a)^2\right]^{1/2}} \tag{11}$$

We can now compute the value of the free-space wavelength and the guide wavelength for each sampled frequency, and compare it with the measured wavelength. The width of the waveguide can be computed using nonlinear least squares fitting, but we measured it using a caliper as a = 2.27584 cm. The result is tabulated below. It should be very obvious that our model's predicted values and the measured values is very close to each other.

---

[2]The velocity at which the modulation of the wave propagates through space.

| Frequency (GHz) | Free-Space $\lambda$ (cm) | Predicted $\lambda_g$ (cm) | Measured $\lambda_g$ (cm) |
|---|---|---|---|
| 8294 | 3.61 | 5.958 | 5.89 |
| 8713 | 3.44 | 5.264 | 5.25 |
| 9296 | 3.22 | 4.576 | 4.53 |
| 9792.5 | 3.06 | 4.142 | 4.18 |
| 10296 | 2.91 | 3.792 | 3.77 |
| 10739 | 2.79 | 3.538 | 3.52 |

If we take the limit of equation 11 as $\lambda$ goes to $2a$, we find that the guide wavelength $\lambda_g$ goes to infinity. This corresponds to the velocity going to infinity as well (Figure 1 hints at this), and is known as the cut-off wavelength. That is, any wavelength longer than that will not be passed at all by the waveguide. Since we know that the cut-off wavelength is $2a$, we can conclude our discussion by calculating the cut-off frequency for our waveguide:

$$\lambda_{cutoff} = 2a = 4.55168\,cm = 6.590\,GHz \tag{12}$$

### 2.5.   Conclusion

We started by looking at a slotted line and determined the velocity of electromagnetic waves inside it is very close to the speed of light (c) in a vacuum. We examined its response to different matches by having the end of the slotted line be open, shorted, well-matched and ill-matched and found that the velocity is independent of frequency, and that the VSWR is the lowest when we have a good match between impedance of the cable and resistance (and/or impedance) of the load. We examined a flexible coax cable and found that the velocity of propagation is much slower in this case, important knowledge for designing our experiments. Our last study was focused on waveguide, where we found three interesting results concerning standing waves, velocities and frequency characteristics of the guide. A mismatched load on a coax cable causes a higher standing wave ratio - the same effect happens in a waveguide when we short the end of the waveguide, much accentuated. In measuring the nulls caused by standing waves in a waveguide, we end up calculating the phase velocity, not the group velocity, which is why we found velocities higher than the speed of light for the propagation through the waveguide. The envelope of the wave is not actually traveling at that speed, rather it is as if we intercept the waves at an angle, measuring a velocity much faster than the wavefront actually moves. Finally, we discovered the important characteristic of waveguides to not pass any frequencies below a certain limit - the cut-off frequency.

## 3.  SINGLE SIDEBAND MIXERS AND COMPLEX FOURIER TRANSFORMS

In the first lab at the beginning of the semester we examined double sideband mixers in detail. We now continue that examination, and extend it to consider the leakage power that Fourier transforms contain, and the capabilities of single-sideband mixers to resolve exact frequency values and indicate whether the incoming signal was in the upper sideband or the lower sideband.

### 3.1.  Hardware

We can build both a single sideband and a double sideband mixer out of a configuration of two double-sideband mixers fed with slightly different versions of the input signal. The important part of the single sideband mixer is a phase shifter that creates a 90 degree phase shift in one of the two inputs. The *Quadrature Hybrid* is what we use in the actual data-taking later on, but the same effect can be accomplished through using a cable that is of length $\frac{\lambda}{4}$. When we introduce the phase shift, the two inputs correspond to the two sidebands. The schematic for the single sideband mixer looks like 2
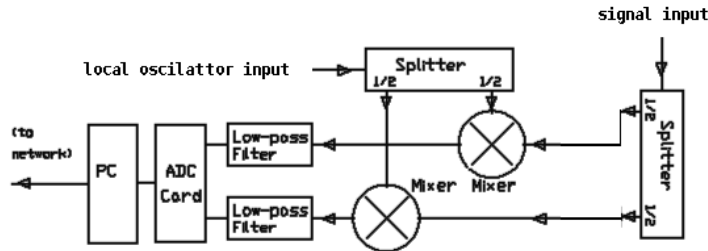


Fig. 2.— The schematic detailing the construction of the single-sideband mixer.

### 3.2.  Dual Sideband Mixer

We used a double-sideband mixer to mix a local oscillator frequency with a signal frequency slightly offset from the local oscillator. In that case we found that the output generated by the mixer is the signal shifted such that the local oscillator frequency corresponds to the DC signal. We modeled the DSB mixer with a local oscillator input of frequency $\omega_0$ and a signal input of $\omega_0 \pm |\delta\omega|$ as follows:

$$E_s \cos\left[(\omega_0 \pm |\delta\omega|)t\right]\cos\left[\omega_0 t\right] \quad = \quad \frac{E_s}{2}\left(\cos\left[\pm|\delta\omega|t\right] + \cos\left[(2\omega_0 \pm |\delta\omega|)t\right]\right) \tag{13}$$

There is a certain ambiguity in the signs in this equation, which we happily ignored, since a property of Fourier transforms made it irrelevant. We found that our power spectra contained the signal at $\pm|\delta\omega|$. Thus, we were left with the ambiguity around the actual value of a received signal - we could at best distill the power spectra peaks to one of two values. This was fine, and a product of the Fourier transform. Fourier Transforms has the following property concerning real signals:

$$x(t) \quad \in \quad \mathbb{R} \tag{14}$$
$$|X(i\omega)| \quad = \quad |X(-i\omega)| \tag{15}$$

Thus, for any real signal, the Fourier transform will be symmetric around the x axis.

Starting off with no phase delay between the mixers, we take two sets of data to investigate the frequency content given by the dual-sideband configuration of our mixer. For both sets, $\nu_{lo} = 11.5MHz$. For the first set we took $f_s = f_{lo} - \delta f$ and for the second set we took $f_s = f_{lo} + \delta f$ with $\delta f = 0.1MHz$. For both these spectra we sample at 10MHz after passing the mixed signals through a bandpass filter. The power spectra are given in figure 3. Looking at the power spectra alone, it is impossible to distinguish between the upper and lower sidebands.
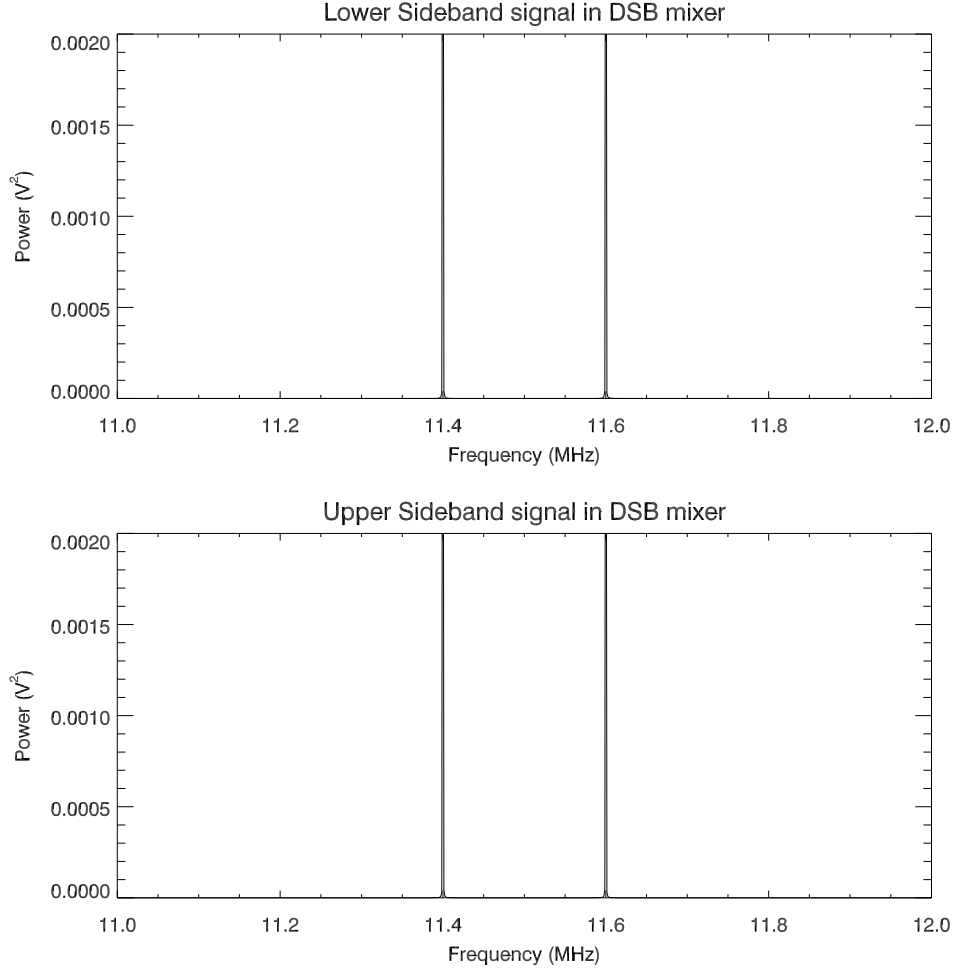


Fig. 3.— The power spectra for the same signal first in the lower sideband $f_s = f_{lo} - \delta f$, then in the upper sideband $f_s = f_{lo} + \delta f$, mixed by a DSB mixer. The frequency spectra appears the same in both cases.

### 3.3.  Leakage Power

Spectral Leakage is the effect of contaminating the power at one frequency in the power spectrum by all the other frequencies in the spectrum. This is a direct result from the non-infinity sampling durations for our Fourier transforms. This causes the Dirac deltas - signals with no width, infinite height and an area of 1 that can be used to describe any signal - to be replaced by functions that are not infinitesimally wide. Power spreads out over the range of these functions, which often takes the form of a sinc function. Thus power "leaks" away from the true frequency into its neighbors.

To examine this we take two sets of data in a setup similar to the experiment we just discussed in section 3.2. First we sample a signal with a frequency that is an integer multiple of the Nyquist frequency $f_N$, then we change the signal to have a frequency that is half an integer multiple of the Nyquist frequency, and we sample again. We take the power spectrum for both cases, which we show in Figure 4. In terms of our previously established nomenclature, we can write:

$$\delta f_1 \quad = \quad \frac{f_N}{2^{M-1}} \tag{16}$$

$$\delta f_2 \quad = \quad \frac{0.5 f_N}{2^{M-1}} \tag{17}$$
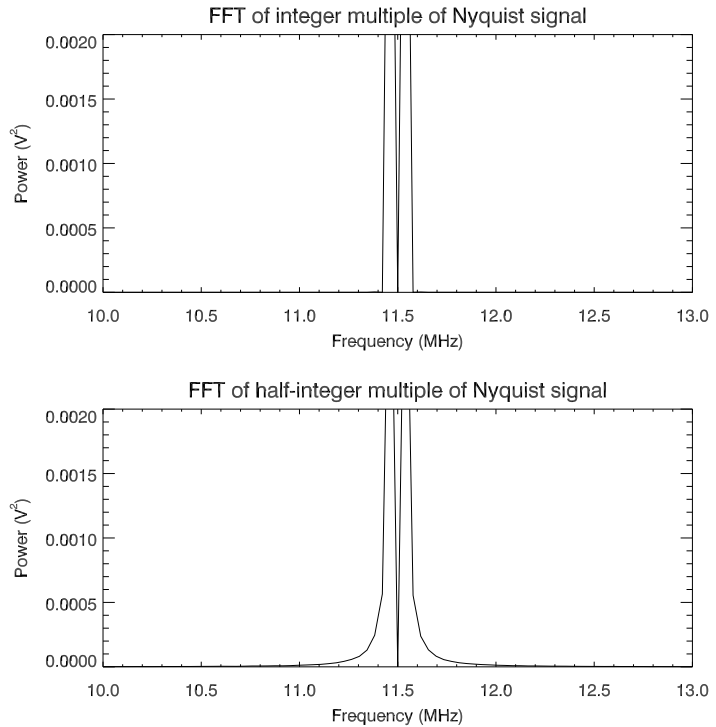


Fig. 4.— The power spectrum of a signal with a frequency that is an integer multiple of the Nyquist frequency and its apparent lack of spectral leakage, versus the power spectrum of a signal with a frequency that is half an integer multiple of the Nyquist frequency and the spread out distribution of power caused by spectral leakage.

It is interesting to find that the leakage power is apparent in the tapered-off power spectrum for half-

integer multiples of the Nyquist frequency, while the integer multiple signal seems to have none of this. Since leakage power is a phenomenon of Fourier transforms, we suspect the explanation to be in the mathematical description of the Fourier Transform:

$$\lim_{T \to \infty} \frac{1}{2T} \int_{-T}^{+T} E(t)e^{2\pi i \nu} dt \tag{18}$$

We only have a limited amount of samples, so no matter how much we wish to integrate with T as infinity, we only cover our sample set. If we do not have an integer multiple of samples, this integral will integrate with a box over multiple samples at once, causing spill into adjacent frequencies for each calculated frequency.

Leakage power can occur for signals at an integer multiple of the Nyquist frequency too. To demonstrate this, we take a DFT with 2048 points of our signal that has an integer multiple of the Nyquist frequency as its peak frequency.
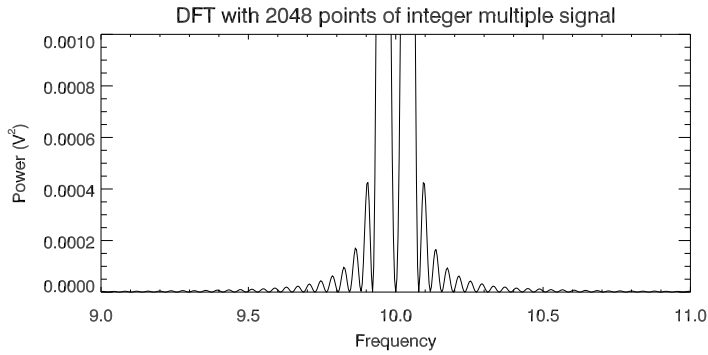


Fig. 5.— The DFT over 2048 points (while we only sampled 256) of a signal with a frequency component equal to an integer multiple of the Nyquist frequency. The leakage power is obvious.

Again we see the phenomenon of leakage power, even more accentuated than in the previous examples. This limits the resolution of our frequency plots, since taking more points hits an upper limit where we only increase the spillage without resolving more information. This frequency resolution - the closest two lines can be next to each other and still be resolved - is the distance equal to apparent width of our lines in Figure 5 and 4, the inverse of the duration of sampling $\frac{1}{T}$

### 3.4. Single Sideband Mixer

We need the capability to distinguish which sideband an incoming signal is in. This information allows us to calculate interesting properties of our objects, for example, the direction of movement relative to us, which we do in section 4 with the Hydrogen line. The Single Sideband mixer promises this capability. We introduce a phase shift of 90° or $\frac{\lambda}{4}$ between the two signals going to the two mixers that make up the SSB mixer. Now, if the signal is in the upper sideband, the one mixer will be $\frac{\lambda}{4}$ before the other mixer, and if the signal is in the lower sideband, the same mixer that was in front will now be shifted by $\frac{\lambda}{4}$ after the other. This allows us to determine, after we calibrate our system with a test signal, which sideband an incoming signal is, and its exact frequency.

We use exactly the same setup as in section 3.2, except we introduce a phase shift by using a cable of length $\frac{\lambda}{4}$ between one of the mixers and the power splitter that splits the original signal into two, one for each mixer. We perform the same experiment, sampling a signal in the upper sideband and a signal in the

lower sideband. We take the power spectrums and plot it in figure 6. Compare this with figure 3 and the power of the single sideband mixer should be very apparent.
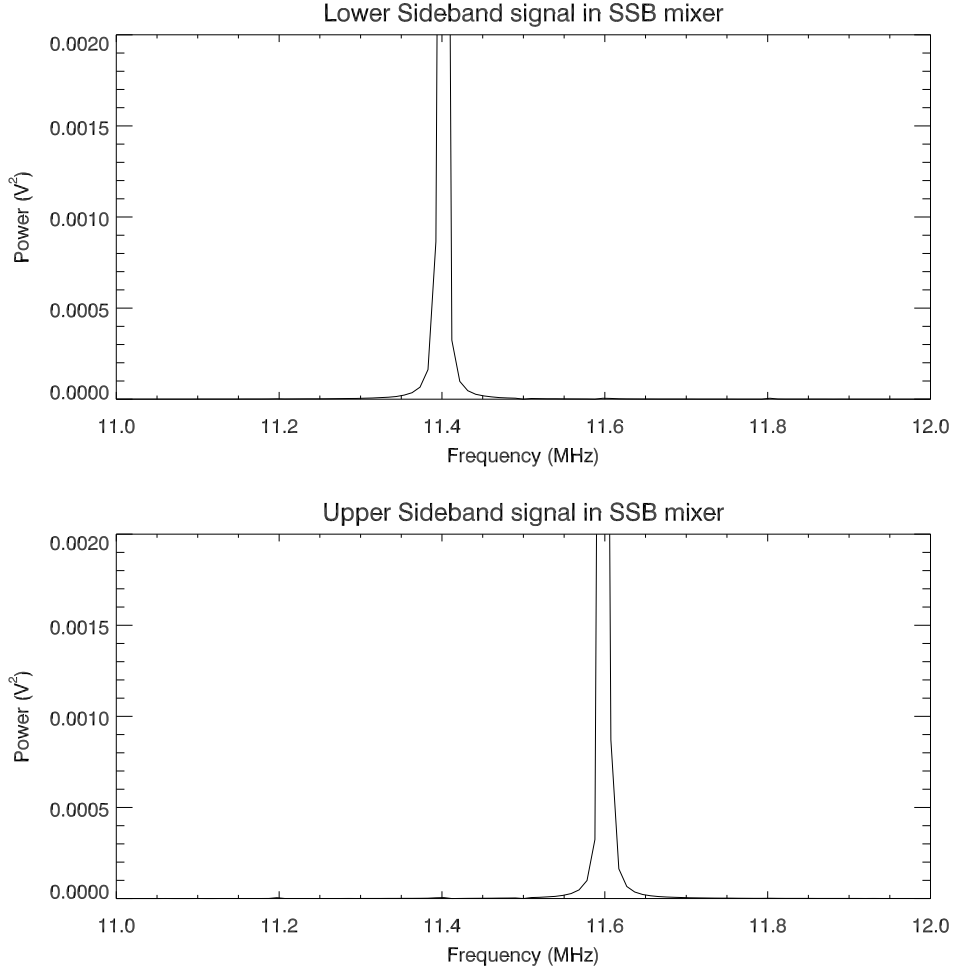


Fig. 6.— The power spectra for the same signal first in the lower sideband $f_s = f_{lo} - \delta f$, then in the upper sideband $f_s = f_{lo} + \delta f$, mixed by a SSB mixer. The true frequency of the input signal is the only frequency present!

## 4.  21-cm LINE ASTRONOMY

### 4.1.  Introduction

We are going to study the 21-cm line emitted by Hydrogen, using all our new knowledge of single sideband mixers to get definite answers for the velocity our object is moving relative to us. To accomplish this, we point a Horn at the galactic coordinates of the object we wish to observe. Our sampled data is reduced and calibrated using several sets of measurements, to finally produce two graphs of the Hydrogen line, one against the observation frequency, one against the Doppler velocity. Thus we find the receding speed of the object, and the intensity of the emission in terms of Temperature[3]

### 4.2.  Experiment

We want to observe the Hydrogen line at 1420.4058 MHz in the region of our Galactic Plane $(120°, 0°)$ galactic coordinates. First, let us consider what information we need to collect. The fact that we want to observe the spectrum around 1420 MHz should serve as a starting point for the data we need to collect. This it not all, though, since we want to calibrate our spectra so that they give an accurate reading of the specific intensity of the source. To accomplish this, we somehow need to get a relative scaling for the power of the incoming signal, so that we can assign a useful value to the voltages we sample. We must also keep into account that our signal path itself will introduce noise, which we want to account for. We can account for all these requirements by making three sets of measurements:

- *SonlineCaloff* Spectrum containing Hydrogen line.

- *SofflineCaloff* Spectrum not containing the Hydrogen line.

- *SofflineCaloff* Spectrum not containing the Hydrogen line with artificial noise of a known intensity inserted into the signal path.

Combining these three sets can, through analysis, supply us with a calibrated X-axis for our spectra.

The signal is feeded through a signal path and into our Digital-Analog Converter so that we can sample it. We prepare our setup through a controlled bench experiment to determine our single-sideband mixer orientation, to ensure that the frequency increases in the direction we believe it to. We did this by generating a signal at 1420 MHz across a wire acting as antenna in front of the horn.

#### 4.2.1.  Signal Path

The signal path for the horn receiver is displayed in Figure 7. The incoming signal, after passing through a bandpass filter that passes 1220 to 1630 MHz, is initially mixed with the first local oscillator in a double-sideband mixer. With a local oscillator frequency of 1610 MHz, the Hydrogen line at 1420.4 is mixed down to $1610 - 1420.405 = 189.595$ MHz and $1420.405 - 1610 = -189.595 Mhz$. This is passed through another bandpass filter (Centered at 190MHz, bandwidth of 22MHz) and into the single sideband mixer. Here it is mixed with 190 MHz. The output is finally filtered through two 5MHz low-pass filters and sampled. Thus the final frequency spectrum is centered at $1610 - 190 = 1420$ MHz with the Hydrogen line at $1420 + 0.405 = 1420.405$ MHz.

#### 4.2.2.  Data

We first convert the Galactic Coordinates $(120°, 0°)$ to an right ascension and declination value, which we can easily convert to the azimuth and altitude of this point in the Galactic Plane for our observation.

---

[3]We measure intensity on the Kelvin scale, as all astronomers do
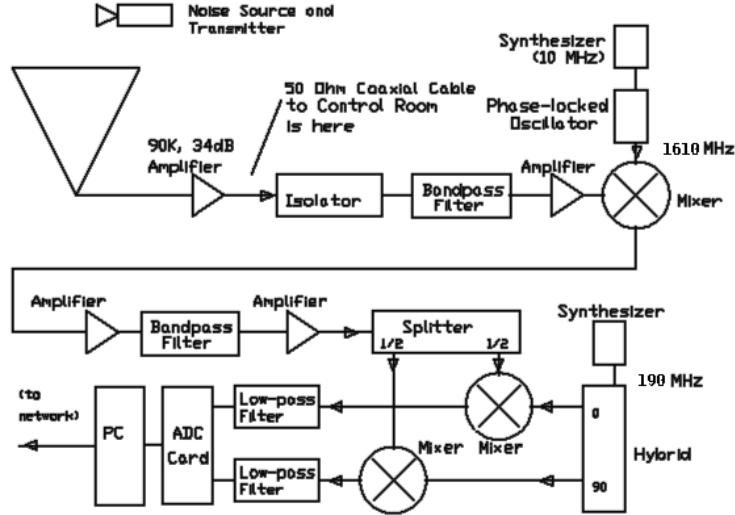
Fig. 7.— The block diagram for the receiver system and signal path of the 21-cm horn.

$$(l, b) \quad = \quad (\alpha, \delta) \tag{19a}$$

$$(120°, 0°) \quad = \quad (0h\, 26m\, 48s \, , \; 62°\, 48m) \tag{19b}$$

We take 100 datasets, each of 262144 samples, for each of the three observations listed in section 4.2. For just one set, we see a large amount of random noise, and some strong peaks from DC noise that the mixers and amplifiers creates in our signal path. By averaging over 100 datasets, we decrease the noise by a factor of 10, since noise goes according to $\frac{1}{\sqrt{n}}$. We remove and interpolate over the strong interference/noise peaks visible in figure 8, where we depict the averaged, raw data from the horn. This procedure of extraction of the useful information from a noisy signal by using multiple datasets is beautifully illustrated in an animation using this data that shows each consecutive averaging as a frame in the animation. This animation is available at **http://ugastro.berkeley.edu/~njoubert/** under "Lab 3 Excerpts".

15
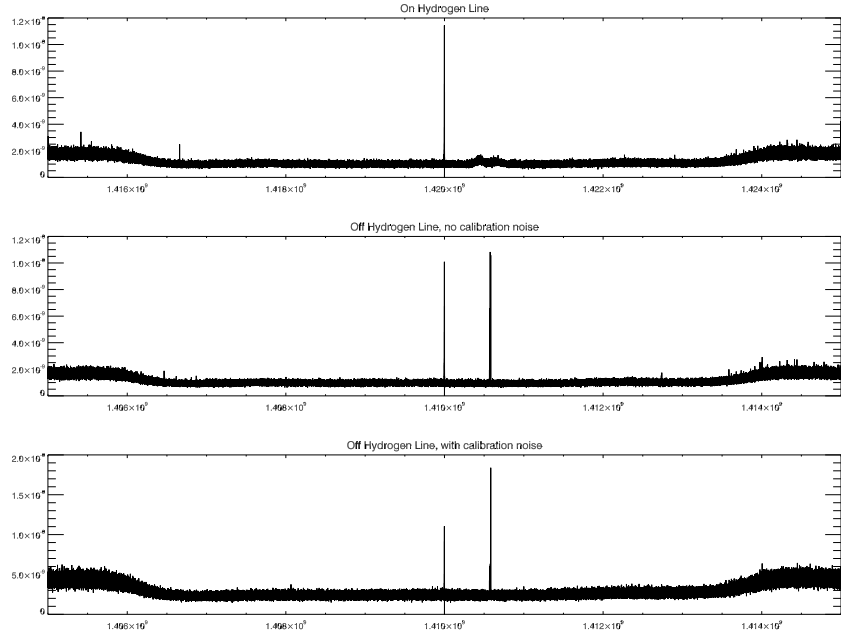
Fig. 8.— Three sets of raw data from 21-cm observations with Horn. Notice the strong interference peaks, especially at the center of the observation range, which corresponds to a DC spike caused by our dual-sideband mixer.

The effect of interpolating over the two strong interference peaks, and the relative levels of our three measurements is shown in figure 9. The observation with artificial noise inserted is significantly stronger than the other two observations, as can be expected. The observation that contains the 21-cm line has the line visible around the center of our frequency range.
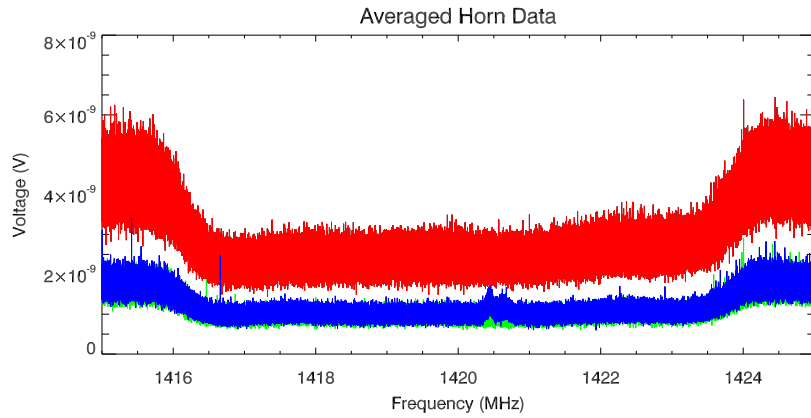


Fig. 9.— The online spectrum after interpolating over the interference peaks.

16

### 4.3. Data Analysis

The first curios aspect of the spectra that we need to address is the initially unexpected *increase* in signal strength more than about 4 MHz away from the center frequency (1420 MHz). The explanation for this can be found in our signal path (discussed in section 4.2.1). We sample at 10 MHz, which means our total bandwidth in 10 MHz. Any signal more than 5 MHz away from the center frequency will be aliased in the sampling process. We try to prevent any signal with a frequency more than 5MHz off center from entering the sampler by using to 5MHz low-pass filters. This setup seems perfect on first glance, but we need to take into account the effectiveness of the low-pass filters. Our claim that it only passes signals below 5MHz is not completely true. A more accurate way of stating the effect of the 5MHz low-pass filters is:

Any signal above 5MHz will be attenuated with more than $\frac{1}{\sqrt{2}}$ of its original value.

Thus there is still some signal coming through at 5MHz and higher, and those parts of the spectrum is aliased, and the aliased signals add up to create what appears to be an increase in intensity of the noise, while it turns out to be only an artifact of out signal path.

Since this section of the spectrum contains no useful information, we can safely truncate that part of the spectrum away. We do this to all 3 datasets, and smooth the power spectrum using a box average with a width of 500 samples. This smoothing results in a frequency resolution of:

$$resolution = \frac{(frequency\,range)*(window)}{(nr\,of\,samples)} = \frac{(10^7)(200)}{262144} = 7.6KHz \qquad (20)$$
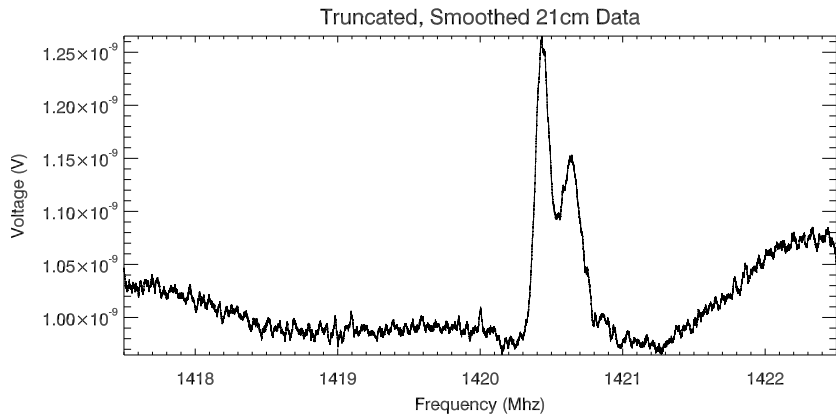


Fig. 10.— Truncating off the aliased sections of our data and smoothing it with a box of width 500 produces an excellent outline of the hydrogen line. Notice that the baseline has wide fluctuations over the frequency range.

This spectrum looks pretty impressive overall, with a very distinct peak for the Hydrogen line. Unfortunately the shape of the noise itself can be seen to fluctuate across the frequency axis, so our main peak itself is probably also slightly distorted from the noise and other affects. This contorted shape is caused by the *Instrumental Bandpass* - the varying effect of our signal path to boost or attenuate the signal. We can remove this by taking a ratio between the spectrum that contains the hydrogen line and the spectrum that contains only noise.

$$ratio = \frac{S_{online}}{S_{offline}} \qquad (21)$$

17

We now have the correct shape of the line, but the y-axis is still in terms of voltage. We want to calibrate our spectra in terms of intensity. This is where we use our other measurement, where we inserted noise of a known amount into the system. To get the line intensity in terms of the calibration noise source, we first calculate the system temperature $T_{sys}$:

$$T_{sys} = \frac{\sum S_{offline}}{\sum (S_{offline,calon} - S_{offline})} T_{sys} \tag{22a}$$

We now have a value by which we can calibrate our spectra so that their y-axes are the intensity in terms of Kelvin though a simple multiplication. We found that $T_{sys} = 329.9$ Kelvin.

$$calibrated\,spectrum = ratio * T_{sys} \tag{23a}$$
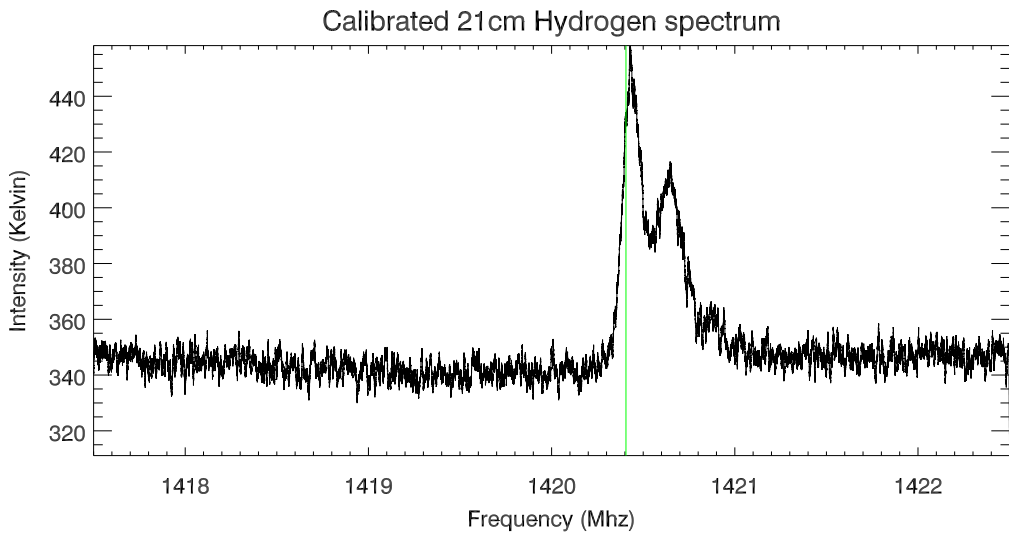


Fig. 11.— The calibrated 21-cm line spectrum plotted against frequency.

Our calibrated spectrum is thus shown in figure 11. We can see that our background noise is around 350 Kevin, and the Hydrogen line peaks at 450 Kelvin. The two peaks are situated at 1420.436 MHz and 1420.650 MHz.

### 4.3.1. Velocity and Doppler correction

We can plot the velocity as given by the Doppler effect using the straightforward Doppler equation formula

$$\frac{\nu}{c} = -\frac{\Delta f}{f_0} \tag{24}$$

where $f_0 = 1420.4058$ MHz, the rest frequency of the 21-cm Hydrogen line. The result of this can be seen in figure 12. This is not the end of the data analysis though, since we have not accounted for the Doppler shift due to the earth's movement to these values. In doing so, we find that the Doppler correction for this point (Eq. 19a) in the sky on Julian day 2454194.3[4] is $0.616 \frac{km}{s}$, which we subtract from our calculated

---

[4]We took our data at Noon PST on Apr 03 2007

18

Doppler velocities, to create figure 13. From here we find that the two peaks move at -6.5 km $s^{-1}$ and -52.05 km $s^{-1}$ away from us. These two values correspond to two spiral arms of our galaxy, the faster-moving one being the arm that is further away, and the slower-moving one being the one we are in.
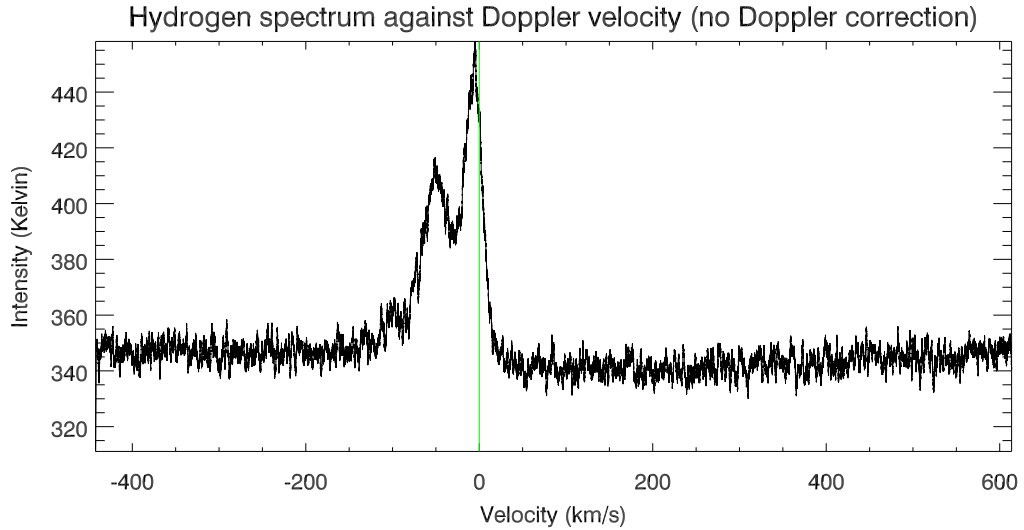


Fig. 12.— The calibrated 21-cm line spectrum plotted against the Doppler velocity, with no corrections for the Doppler shift of the observations due to the Earth's relative movement.
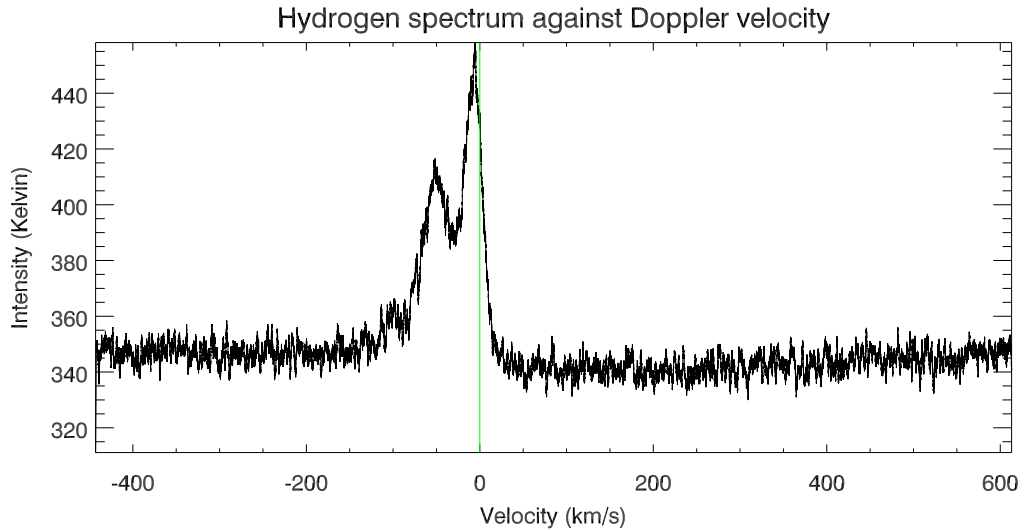


Fig. 13.— The calibrated 21-cm line spectrum plotted against the Doppler velocity, corrected for the Doppler shift of the observations.